arXiv:1611.05918v1 [q-bio.NC] 17 Nov 2016

Morphology of Fly Larval Class IV Dendrites Accords with a Random Branching and Contact Based Branch Deletion Model.

Sujoy Ganguly[1], Olivier Trottier[1], Xin Liang[2], Hugo Bowne-Anderson[1], and Jonathon Howard[1]

[1]Department of Molecular Biophysics and Biochemistry, Yale University, New Haven
[2]Tsinghua-Peking Joint Center for Life Sciences, School of Life Sciences, Tsinghua University, Beijing, China

November 21, 2016

Abstract

Dendrites are branched neuronal processes that receive input signals from other neurons or the outside world [1]. To maintain connectivity as the organism grows, dendrites must also continue to grow. For example, the dendrites in the peripheral nervous system continue to grow and branch to maintain proper coverage of their receptor fields [2, 3, 4, 5]. One such neuron is the *Drosophila melanogaster* class IV dendritic arborization neuron [6]. The dendritic arbors of these neurons tile the larval surface [7], where they detect localized noxious stimuli, such as jabs from parasitic wasps [8]. In the present study, we used a novel measure, the hitting probability, to show that the class IV neuron forms a tight mesh that covers the larval surface. Furthermore, we found that the mesh size remains largely unchanged during the larval stages, despite a dramatic increase in overall size of the neuron and the larva. We also found that the class IV dendrites are dense (assayed with the fractal dimension) and uniform (assayed with the lacunarity) throughout the larval stages. To understand how the class IV neuron maintains its morphology during larval development, we constructed a mathematical model based on random branching and self-avoidance. We found that if the branching rate is uniform in space and time and that if all contacting branches are deleted, we can reproduce the branch length distribution, mesh size and density of the class IV dendrites throughout the larval stages. Thus, a simple set of statistical rules can generate and maintain a complex branching morphology during growth.

In our brains, billions of neurons interact with each other to build a nervous system of unparalleled complexity and computational power. Neurons have dendrites, which are branched structures that receive synaptic or sensory inputs, and an axon, which send outputs to other neurons. The shape or morphology of individual neurons sets the number and types of interactions that a neuron can have and provides the structural basis of neuronal computation [9, 10, 11, 12, 13, 14].

Since many organisms continue to enlarge after the establishment of the body plan, it is critical for axons and dendrites to maintain their morphology as they grow. For example, interneurons of the grasshoper [2], motor neurons in moths [3] and mice [4] grow drastically in size yet maintain connections to their target cells. Futhermore, dendrites in the perpherial nervous system, like those of gold fish retinal ganglion cells [5], and dendritic arborization (da) sensory neurons of the fly larva [6], which are the subject of this work, grow to continually maintain coverage of their receptor fields. In this paper, we investigate the growth rules that are required to maintain the correct branching morphology as a dendrite grows.

The da sensory neurons of the fly larva are a model system for studying dendritic arborization [15, 16, 17]. These dendrites innervate the extracellular matrix, which lies between the outer cuticle and the inner epidermal cell layer [7]. They tile the surface on the fly larva in a highly stereotyped manner and have four distinct morphological classes [18] (Fig. 1 A). Since it is easy to identify and image individual da neurons, these neurons have proven to be a powerful model system for studying dendrite morphology [15, 16]. In this paper, we address the question of how the morphology of the class IV da neurons (Fig. 1 B) is maintained during the larval stages.

The class IV da neuron has highly branched dendrites [18], which detect potentially harmful stimuli, such as the ovipositor barb of parasitic wasps [8, 19]. The dendrites of the class IV neuron begin

morphogenesis during late embryogenesis ~ 16 hrs After Egg Lay (AEL). By the time the larva hatches (~ 22 hrs AEL at 25 °C), the class IV dendrites nearly cover its surface. The dendrites then continue to expand and branch as the larva grows ($22 - 126$ hrs AEL), so that the neuron maintains its coverage of the larval surface [6].

In this work, we are seeking the growth rules that allow class IV dendrites to maintain their dense coverage of the larval surface. To this end, we have used a novel measure, the hitting probability, that quantifies the mesh size and two well-known measures of branching morphology: the fractal dimension [20] and lacunarity [21, 22] (see Definition of Morphometrics). We show that these measures remain largely invariant over larval stages, despite a several fold increase in larval length. Furthermore, we demonstrate that a model with simple rules for branching and self-avoidance can capture essential features of the establishment and maintenance of the dendrite's morphology.

1 Experimental Results

To characterize the morphology of fully-developed class IV dendrites, we imaged larvae expressing Cd4-tdGFP under the ppk promoter (*ppk-cd4-tdGFP*) during the third instar stage (Fig. 1) using a laser-scanning confocal microscope (See Material and Methods for details). Using NeuronStudio [23] and Fiji we traced the branches of the dendrites to produce skeletons. These skeletons were then analyzed to obtain the the mesh size, density and uniformity of class IV dendrites using parameters defined in the next section.

Definition of Morphometrics

Here we include simple definitions of the relevant morphometrics to aid comprehension.

Hitting Probabiltiy $H(B)$: The probability that a box of size B hits the dendrite.

Mesh Size B_{H}: The length at which 50% of all boxes hit the neuron.

Fractal Dimension d_{f}: A measure of the space-fillingness of a shape. For a completely filled box $d_{\mathrm{f}} = 2$, for a straight line $d_{\mathrm{f}} = 1$, for branched shapes $1 \leq d_{\mathrm{f}} \leq 2$.

Lacunarity $\Lambda(B)$: A measure of density fluctuations as a function of length scale B.

Lacunarity Length B_Λ: The length at which $\Lambda(B = B_\Lambda) = 0.25$, i.e. the length at which the neuron is uniform. The larger B_Λ, the more variable the density of the neuron.

Radius of Gyration R_{g}: A length scale that measures how spread out a shape is from its center. The larger R_{g} the more spread out the neuron.

Persistence Length β: The characteristic length at which a branch bends.

For mathematical definitions see **Appendix**.

1.1 Class IV dendrites have a small mesh size

To characterize the mesh size of the dendrites, we developed a novel measure called the hitting probability $H(B)$. $H(B)$ measures the probability H that a randomly placed box of size B hits the dendrite (see Appendix for details). The hitting probability generalizes an earlier metric called the coverage index [6] by allowing for any box location and any box size. A typical hitting probability curve of a neuron (Fig. 1 D) $H(B)$ increases monotonically with B, eventually reaching $H = 1$ as B approaches the size of the neuron.

We define the characteristic mesh size B_{H} as the box size at which half of all boxes hit the dendrite. In other words, B_{H} is the maximum size of a stimulus that would go untouched, or undetected, on average, by the neuron. B_{H} is similar to the mesh size in a cross-linked polymer network[24].

We found that $B_{\mathrm{H}} = 8.4 \pm 0.5\,\mu\mathrm{m}$ (mean $\pm$ SD, $n = 14$ neurons) for the mature dendrites of the class IV neuron. Thus, the mesh size is approximately equal to the diameter of the ovipositor barb of wasps that lay eggs in *Drosophila* larva ($\sim 10\,\mu$m, [8]). This indicates that the class IV dendrite has a high chance of detecting a wasp attack. Furthermore, the mesh size is small compared to the overall size of the neuron ($\sim 500\,\mu$m) and is similar to the mean branch length (see below).

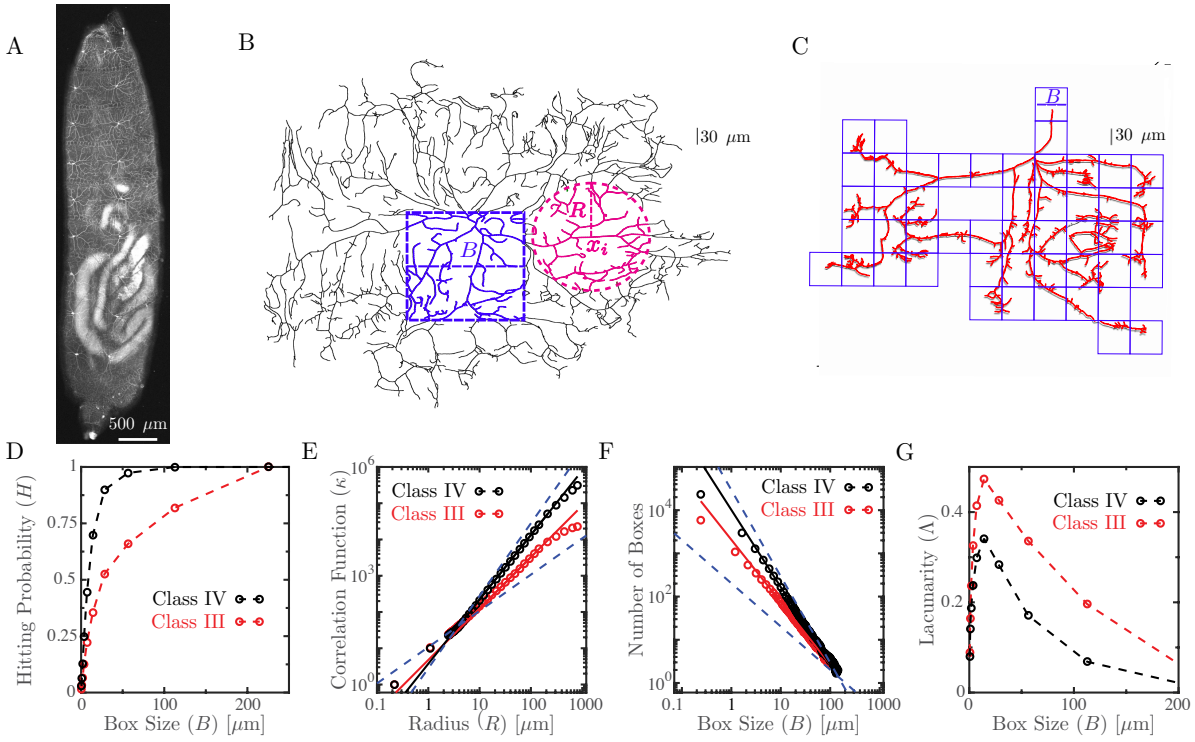

Figure 1: **Morphometrics of class IV and class III dendrites. (A)** 3rd instar larval expressing GFP-tagged membrane protein (*ppk-cd4-tdGFP*) in class IV neurons. **(B)** The skeleton of a class IV neuron from a third instar larva with an example of a box used to calculate the hitting probability (blue) and a circle used to calculate the correlation dimension d_c (magenta). **(C)** The skeleton of a class III neuron from a third instar larva with an example of a set of boxes used to compute the box dimension d_b and lacunarity function Λ. See **Definition of Morphometrics** and **Appendix** for details **(D)** Example hitting probability H versus box size B. **(E)** The correlation function κ versus the radius R. Fits used to determine the correlation dimension d_c plotted in solid lines. See **Appendix** for details of fits. The curves for $d_c = 1$ and $d_c = 2$ are plotted in blue for reference. **(F)** The number of boxes needed to cover a neuron versus the box size B. Fits used to determine $-d_b$ are plotted in solid lines. See **Appendix** for details of fits. The curves for $d_b = 1$ and $d_b = 2$ are plotted in blue for reference. **(G)** Lacunarity function Λ versus box size B for a class IV neuron (black) and a class III neuron (red).

1.2 Class IV dendrites are dense and uniform

To understand the morphological basis underlying B_H we quantified the density and uniformity of the class IV dendrites during the third instar stage. The fractal dimension d_f is a commonly used measure of how a branched structure fills space. A solid square, for example, has a $d_f = 2$, while a straight line has a $d_f = 1$ (See Appendix for mathematical definitions of d_f). We found that the fractal dimension of class IV dendrites was $d_f = 1.80 \pm 0.04$ (mean $\pm$ SD, $n = 14$), indicating that the dendrites are dense and space filling.

To establish a small mesh, a dendrite needs to not only be space filling (i.e. $d_f \sim 2$), but uniformly so. To measure the uniformity of the dendritic arbor, we used the lacunarity function $\Lambda(B)$. This measures the density variation as a of function length scale B. To compare the lacunarity of different cells we calculated the length B_Λ ($\Lambda(B = B_\Lambda) = 0.25$ see Definition of Morphometrics). The smaller B_Λ, the more uniform the dendritic density. We found that $B_\Lambda = 32.6 \pm 16.8\,\mu$m (mean $\pm$ SD, $n = 14$) for third instar larva. In other words, on spatial scales larger than $33\,\mu$m the density of the neuron is uniform, whereas below $33\,\mu$m it is variable. While the B_Λ is larger than the mesh size B_H, it is much smaller than the dendrite size, indicating that the coverage is uniform and arbors can be considered homogeneous. In summary (Tab. 1), mature class IV neurons have dense (large d_f) and uniform (small B_Λ) dendritic arbors, which is consistent with a small mesh size (small B_H).

1.3 Class IV dendrites have a tighter mesh, are denser and more uniform than class III dendrites

To assess the ability of these measures to quantify dendritic morphology, we also imaged class III cells (Fig. 1 C). Class III cells are gentle touch sensors and use a different set of mechanotransduction channels [25]. The class III dendrites (Fig. 1 C) are substantially less branched and have smaller branches, on average, than the class IV dendrites (Tab 1). We find that $H(B)$ is much smaller for class III neurons than for class IV neurons (Fig. 1 D) for most box sizes. Consequently, we find that the mesh size B_{H} is much larger in class III neurons ($B_{\mathrm{H}} \sim 24.7\,\mu$m) than in class IV neurons ($B_{\mathrm{H}} \sim 8.4\,\mu$m) (Tab. 1). In other words, class III dendrites have larger gaps in coverage than class IV dendrites.

Table 1: Properties of class IV and class III neurons. All numbers are mean ± SD.

	class IV (n = 14)	class III (n = 8)
Mean branch length, $\langle L \rangle$	$12.54 \pm 0.04\,\mu$m	$7.49 \pm 0.8\,\mu$m
Mesh size, B_{H}	$8.37 \pm 1.80\,\mu$m	$22.7 \pm 4.8\,\mu$m
Fractal dimension (correlation method), d_{c}	1.80 ± 0.04	1.42 ± 0.03
Fractal dimension (box method), d_{b}	1.79 ± 0.04	1.43 ± 0.04
Lacunarity length, B_Λ	$32.6 \pm 16.8\,\mu$m	$130.5 \pm 31.2\,\mu$m

We find that class III dendrites have a fractal dimension of $d_{\mathrm{f}} \sim 1.42$ (Tab 1), which is substantially smaller than the class IV neuron. In other words, class III dendrites are sparser, at all scales, than class IV dendrites (Fig. 1 E and F). We find that the lacunarity Λ decays much slower (with B) for class III dendrites compared to class IV dendrites (Fig. 1 G). Consequently B_Λ is much larger (Tab. 1) for class III dendrites than for class IV neurons (Tab. 1) showing that they are less uniform than class IV neurons. These results (Tab. 1), show that class III neurons are sparser (small d_{f}) and less uniform (large B_Λ) than class IV dendrites, which is consistent with having larger mesh size (large B_{H}). These differences likely reflect the different mechanoreceptor functions of class III and class IV neurons (see Discussion).

1.4 Class IV dendrites maintain a tight mesh, high density and uniformity throughout larval stages

To determine how the morphology of class IV dendrites changes with time, we imaged and skeletonized the class IV dendrites, as before, from early first instar (30 hrs AEL) to wandering third instar (126 hrs AEL) (Fig. 2 A). We used the larval body segment length as a proxy for time since each data point comes from a unique larva, and S increases linearly with time [26] (SI).

The mesh size B_{H} increased modestly from $4.4 \pm 0.3\,\mu$m (1st instar) to $8.5 \pm 1.4\,\mu$m (third instar) (Fig. 2 C). This two-fold increase is less than the six-fold growth in larval body segment size and indicates that the mesh size remains small during development. Interestingly, the ratio between B_{H} and the mean branch length $\langle L \rangle$ is nearly constant during development showing that the shape of the arbor has remarkable conservation during development

The morphologies of the class IV neurons remained dense and uniform during the larval stages of development. We found that the fractal dimension (Fig. 2 D) in the just hatched larvae ($\sim$ 30hrs AEL) was $d_{\mathrm{f}} \sim 1.7$ and increased to 1.75 within 24 hours, eventually rising to about 1.8 during the next four days. The lacunarity slightly increased with time (Fig. 2 E). By rescaling B by the radius of gyration R_{g} (i.e. overall neuronal size see Eq. 1), we found that Λ follows the same curve at all developmental times, i.e., collapses when scaled by R_{g} (Fig. 2 D inset). The nearly constant fractal dimension and the collapse of the lacunarity curves indicate that the morphological pattern of the class IV neurons is mostly established during embryogenesis.

2 Dynamic Model of Class IV Development

The maintenance of a small mesh size throughout larval stages raises the question: how can the class IV dendrites achieve this, despite the six-fold increase in the larval segment size? To answer this question, we developed a mathematical model of class IV dendrite morphogenesis during the larval stages. Our model consists of three rules that determine 1) branch creation, 2) the direction and speed that this new branch grows, and 3) how branches avoid crossing the other branches (self-avoidance).

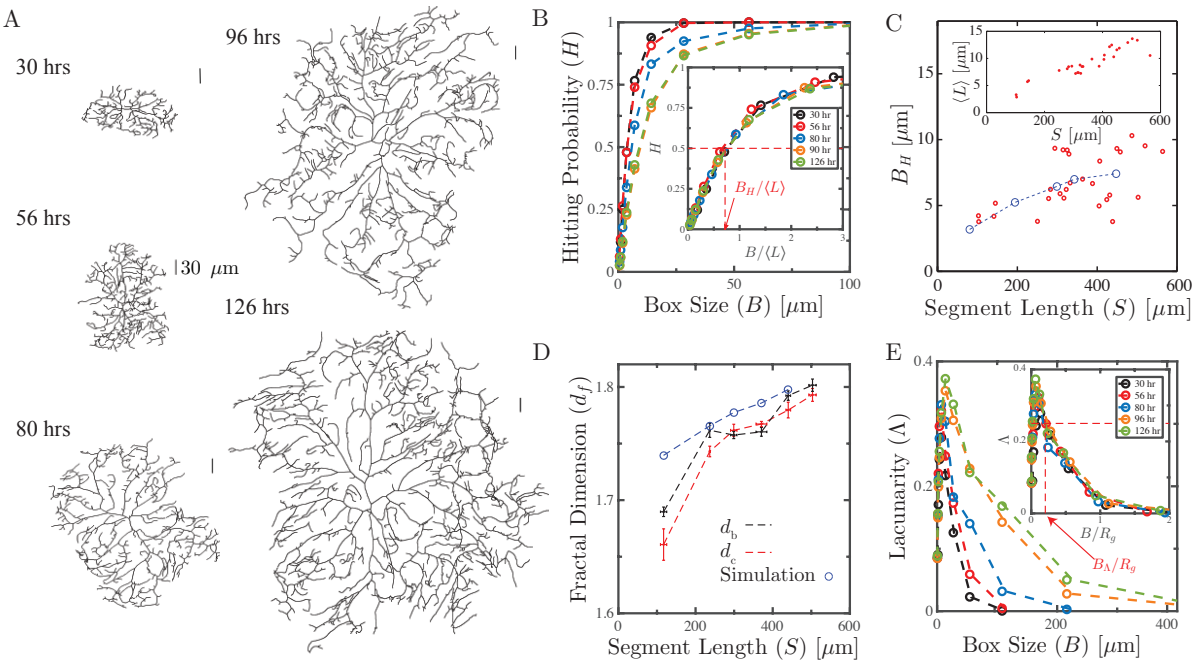

Figure 2: **Morphometrics of class IV neurons during larval growth. (A)**Examples of class IV neurons during larval stages. All scale bars 30 μm, all time stamps hours After Egg Lay. **(B)** The hitting probability H is plotted versus the box size B for the 5 neurons shown in Fig. 2 A. In the inset, we plot H versus $B/\langle L\rangle$. We define the mesh size $B_{\rm H}$ such that $H(B = B_{\rm H}) = 0.5$. $B_{\rm H} \sim 0.72\langle L\rangle$ throughout the larval stages. **(C)** $B_{\rm H}$ is plotted versus larva body segment length S (red 28 cells). For simulated neurons, $\omega = 0.2\,{\rm min}^{-1}$ and $\alpha = 10^2\,\mu$m (blue). In the inset, we have plotted the mean branch length of the class IV dendrites versus the larva body segment length S. **(D)** The fractal dimension $d_{\rm f}$ is plotted against S. We have binned the data by body segment length S with bin widths of 77 μm. Simulation parameters are same as before. **(E)** The lacunarity Λ is plotted against box size B for the five neurons in Fig. 2. In the inset, we plot Λ versus $B/R_{\rm g}$. We define the lacunarity length B_Λ as the box size at which $\Lambda(B = B_\Lambda) = 0.25$.

2.1 Branch Creation

We found that the number of branch points increases with time during larval stages (Fig. 3A), and this increase was well described by a linear function with a net branch creation rate $\omega_{\rm net} \sim 0.1$ branch points min^{-1} (Tab. 2). This observation led us to model branch creation as a time invariant process with a branching frequency ω. Since $\omega_{\rm net}$ can include the removal of branches (see below), it is a lower bound on the branching creation frequency ω.

We also measured the branch length distribution, and found that it was well described be an exponential distribution (Fig. 3 B). Furthermore, we found that that the branch length was independent of the branch depth, defined as the number of branch points between a branch and the soma along the shortest path (Fig. 3 C). Motivated by these observations, we modeled branch creation as a random process that was uniform along the neuron and constant in time.

2.2 Tip Elongation

Since the growth of class IV dendrites occurs at the branch tips [27, 6], we modeled neuron growth as branch tip elongation. We measured the overall size of class IV dendrites using the radius of gyration $R_{\rm g}$ (Eq. 1). $R_{\rm g}$ measures spread of neuron mass from its center. We found that $R_{\rm g}$ increases linearly during development (Fig. 3 D). Therefore, we assume that the tip elongation rate v is constant in time and $v \propto V_{\rm g}$, where $V_{\rm g}$ is the growth speed of the class IV dendrite. The assumption of a constant growth speed assumes that the simulation time scale is much larger than the fluctuation times scale. We estimated $V_{\rm g}$ from the change in dendrite size during development (Fig. 3 D), and found $V_{\rm g} \sim 0.04\,\mu{\rm m\,min}^{-1}$ (Tab 2).

To determine the direction of branch growth, we measured how much the path of a branch changes as a function of path length by using the persistence length β; the distance over which the orientation

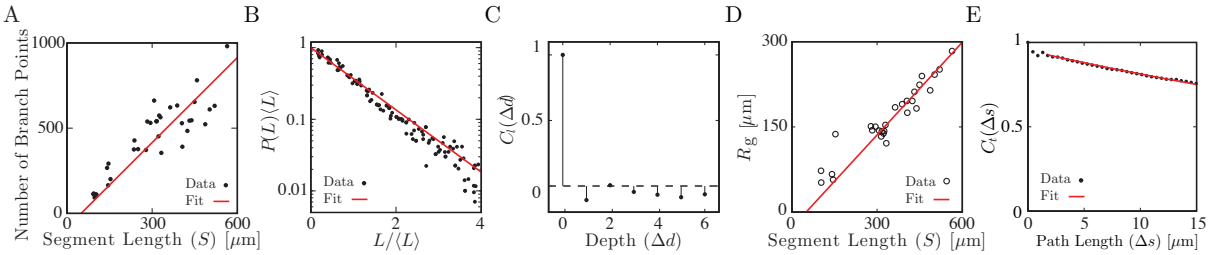

Figure 3: **Branching Rules (A)** Number of branches versus larval body segment length S for class IV dendrites at different larval stages. The slope of the fit is 1.64 branches μm^{-1} for the line passing through the S axis at 50 μm, the segment length at the onset of dendritogenesis. **(B)** The probability density $P(L)$ that a branch of a dendrite (at a particular time) has length L. The probability density is rescaled by multiplying by $\langle L\rangle$ and the branch length is rescaled by dividing by $\langle L\rangle$ (of the particular dendrite). The superposition of the data indicates that the branch lengths are well described be an exponential distribution (red line) at all larval stages. **(C)** The branch length autocorrelation C_l (Eq. 3) vs depth difference Δd averaged over all branches. The near-zero values for $\Delta d \geq 1$ imply that branch length is independent of depth. **(D)** The radius of gyration $R_{\rm g}$ (Eq. 1) of 28 class IV neurons versus larval body segment length S. The slope of the fit is 0.39, where the $S-$intercept is set such that $R_{\rm g} = 0$ at the onset of class IV dendrite morphogenesis. **(E)** The tangent vector autocorrelation function C_t (Eq. 2), averaged over all branches, versus the path length lag Δs (Eq. 2). The red line is an exponential fit to the data $C_t(\Delta s) = e^{\Delta s/\beta}$, where $\beta = 44.8 \pm 1.5\,\mu$m is the persistence length.

of the direction of growth of a branch changes (see Appendix for mathematical details). We find that $\beta = 45 \pm 2\,\mu$m (Tab. 2, Fig. 3 E), which is much greater than the mean branch length ($\langle L\rangle \sim 12.5$ Tab. 1), indicating that branches tend to be straight.

2.3 Self-Avoidance

Previous work has shown that the branches of the class IV neuron do not cross each other. Furthermore, it is known that this self-avoidance is contact mediated and it has been proposed that branches retract after contact [27, 28, 29, 30]. Therefore, we modeled self-avoidance by having growing branches retract at a constant speed v (same as elongation rate), if they contact an existing branch. For simplicity, the retraction length was assumed to be exponentially distributed with a mean retraction length α.

Table 2: Parameters in the model. All errors are SD (n=28 neurons).

Parameter	Measured Value	Simulation Value
Branching frequency	$0.12 \pm 0.03\,\text{min}^{-1}$ ($\omega_{\rm net}$)	$0.01 - 2\,\text{min}^{-1}(\omega)$
Tip elongation rate, v	$0.04 \pm 0.02\,\mu\text{m}\cdot\text{min}^{-1}$	$0.08\,\mu\text{m}\cdot\text{min}^{-1}$
Persistence length, β	$44.8 \pm 1.5\,\mu$m	$70\,\mu$m
Retraction length, α	not measured	$0 - 1000\,\mu$m

2.4 Model Implementation

Using these rules, we arrived at a four parameter model; ω the branch creation rate, v the growth speed, β persistence length and α to retraction scale. We implemented our model on a hexagonal lattice, with lattice spacing $\epsilon = 0.4\,\mu$m. We chose to use a lattice model to facilitate contact detection as the lattice spacing was set to be equal to the thickness of the branches. Since we implemented the rules on a hexagonal lattice, the possible branching angles are limited. Therefore we ignored the role of branching angles on morphology. The lattice spacing and the growth speed act as scale factors, i.e. setting the overall size of the dendrite but not changing the shape. Therefore, we chose v such that the size of a simulated dendrite matched that of a real one, which left us with three free parameters. However, we found that as long as β is large, i.e., as long as the branches are straight, β has little effect on the morphology (SI). Therefore, we focused on how branching frequency ω and the contact-based retraction scale α control the morphology of dendrites.

2.5 Model Results

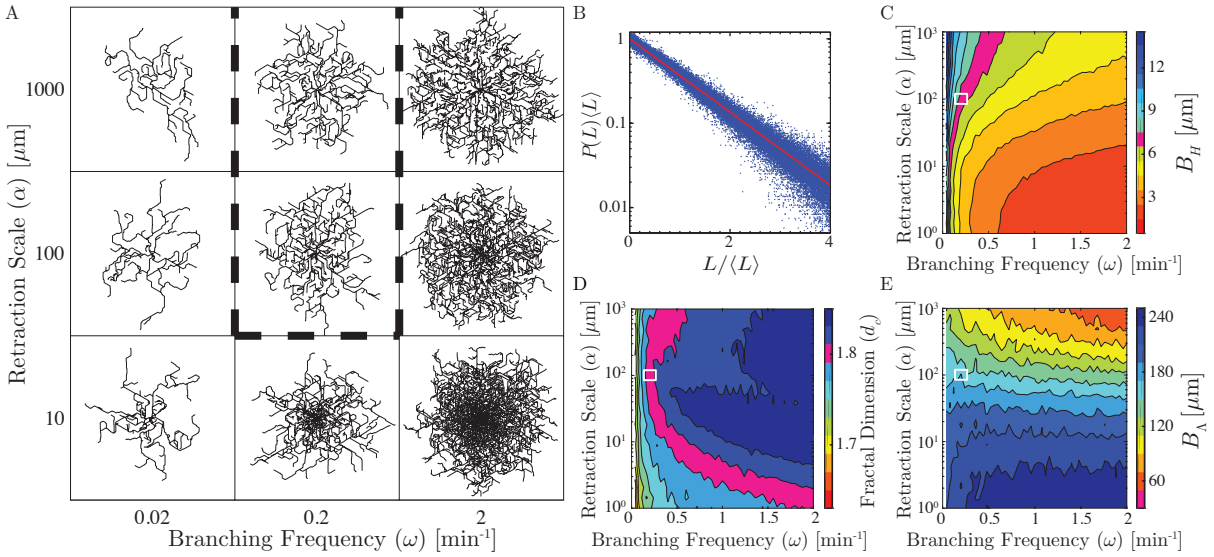

Figure 4: **Simulations of dendritic growth (A)** Nine representative simulations of dendrties for a range of branching frequencies ω and retraction scales α. For all simulations, the persistence length was $\beta = 70$ μm and simulation time was $T = 100$ hrs. For $\alpha \gg 1$ μm and $\omega \sim 0.2\text{min}^{-1}$ (dashed box) we have subjective agreement with the morphology of real neurons. **(B)** The branch length distribution for simulated neurons in the dashed black box in **(A)** is approximately exponentially distributed as observed. **(C)** The mesh size B_H in a contour plot versus the branching frequency ω and retraction scale α. Note that the retraction scale α is plotted in a log scale. In pink we have highlighted the observed value of $B_\text{H} = 7\,\mu$m (see Tab. 1). The white box indicates the values used for the time series plotted in Fig. 2 C and D ($\omega = 0.2\,\text{min}^{-1}$ and $\alpha = 10^2\,\mu$m). **(D)** The fractal dimension d_f in a contour plot versus the branching frequency ω and the retraction scale α. In pink we have highlighted the physiological value of $d_\text{f} = 1.8$ (see Tab. 1) **(E)** The lacunarity scale B_Λ in a contour plot versus the branching frequency ω and the retraction scale α. We highlighted in pink the observed value $B_\Lambda = 33\,\mu$m (see Tab. 1). We find that this value is not found in the range of values used in our simulations.

We generated simulated neurons for a range of branching frequencies ω and retraction scales α (Fig. 4 A) and analyzed their shape. Importantly, we found that the distribution of branch lengths was exponential (Fig. 4 B) and the branch lengths were uncorrelated with branch depth, for a limited range of parameters (dashed box in Fig. 4 A), which agrees with the experimental observations (Fig. 3 B and C).

To test whether our model provides a good description of the morphology, we measured the mesh size, fractal dimension and lacunarity of the simulated dendrites. The mesh size B_H decreased with increasing ω and decreasing α (Fig. 4 C) and appeared to saturate as ω increases. There was a small region of $\omega - \alpha$ space where there was quantitative agreement between the simulated and observed values of B_H (Fig. 4 C, pink). We found, that d_f increased monotonically with ω and saturated for large values of ω. As for B_H, we found a narrow band of $\omega - \alpha$ space where we have a quantitative agreement between the model and the class IV neuron for d_f (Fig. 4 D, pink). Crucially, there was a small region of $\omega - \alpha$ space where the model recapitulated both B_H and d_f (Fig. 4 C and D, white box). Taking values from this small region ($\omega = 0.2\,\text{min}^{-1}$ and $\alpha = 10^2\,\mu$m), we recapitulated the third instar and even found agreement throughout most of the larval development (Fig. 2 B and 2 C). Thus, the model recapitulates both the mesh size and fractal dimension throughout development. It did not recapitulate the lacunarity, which for the parameter values $\omega = 0.2\,\text{min}^{-1}$ and $\alpha = 10^2\,\mu$m was larger than the observed values. In other words, the model arbors are not as uniform as the observed ones (see Discussion). In summary, this model recapitulates most, but not all aspects of the dendritic morphology of class IV neurons.

3 Discussion

Our key experimental finding is that the morphology of class IV neurons, as characterized by the branch length, mesh size, fractal dimension, and lacunarity, remarkably remains constant during development. Indeed, from the early first instar larva (30 hours after egg lay) to the late third instar larva (126 hours after egg lay), as both the segment size and the number of branches increases approximately six-fold, the mean length, the mesh size, and the lacunarity only increase around two-fold and the fractal dimension is almost unchanged. When we normalize the mesh size by the mean branch length, it is virtually unchanged throughout development. Thus, as these cells grow, key aspects of their morphology are invariant, even as the overall size the number of branches increases by nearly an order of magnitude.

As a first step toward probing the mechanism underlying this geometric invariance, we developed a simple computational model for branched morphogenesis. The model assumes that the branching rate is constant over development (consistent with the observed linear increase in the number of branches), that the rate was independent of position and that growing tips retract random, exponentially distributed distance after contacting other branches. The model reproduced many of the key features of the growth of class IV cells including branch lengths, mesh sizes, and fractal dimensions. However, it was unable to capture the lacunarity (the model predicted a higher relative density in the center than was observed, see SI). Importantly, the data constrained the values of the branching frequency and mean retraction distance. Thus, the model provides a framework for understanding the changes in the morphology of these cells during development.

One of our most striking experimental and theoretical findings was that the branching frequency in class IV dendrites was independent of total dendrite length. Naively, we might have expected that the mean number of branches added per unit time would increase with total dendrite length, as the longer the dendrites, the more positions on which branches could form. However, this would have led to an exponential increase in the number of branches, rather than the observed linear increase. Our modeling shows that even if the retraction length is much larger than the mean branch length, an exponential increase in branch length is still observed, and the distribution of branch lengths deviates from the observed exponential distribution (see SI). The constant branching rate suggests that branching is limited by the production of a nucleating factor that is produced at a constant rate. Furthermore, our finding that branching is uniform in space implies that the putative nucleation factor would be distributed widely and uniformly throughout the cell.

We also found that for our model to recapitulate class IV-like morphologies, contact-based retraction needs to lead to complete branch deletion, i.e., the mean retraction distance (α) is much larger than the mean branch length ($\langle L \rangle$). By deleting the branches whose tips collide with other branches, gaps of a size similar to the mean branch length are created and maintained. Also, dense regions where the gap size is less than or equal to the mean branch length will not increase in density. Such overfilling is seen in the simulations for small retraction lengths (Fig. 4 A). Thus, our model constrains both the branching frequency and the retraction distance.

Finally, we note that the mesh size of class IV dendrites, $4 - 8\,\mu$m, is well suited for detecting highly localized nociceptive stimuli such as punctures by the $10\,\mu$m diameter ovipositor barb of parasitic wasps ([8]). This acuity is maintained throughout development. Thus, the small mesh size is consistent with the class IV neuron being a harsh touch sensor. Indeed, the theory of contact dynamics predicts that the indentation h of the surface of an elastic body poked by a probe with a cross-sectional radius R (pushing normal to the surface) is $h \propto F/R$, where F is the applied force [31]. Therefore, the smaller R, the larger h (for a fixed force); the more local the stimuli, the more sensitive to localized forces. Thus the small mesh size suggests that the class IV neuron is well adapted to sensing harsh touch throughout larval stages. In contrast, the class III neuron, a soft touch sensor, would need to capture diffuse stimuli, i.e., the mesh size can be large. Thus, the morphologies of both class IV and class III neurons are well-suited for their mechanosensitive functions.

4 Materials and Methods

Drosophila Stocks

All flies were maintained on standard medium at 23^{o}C. The strain *ppk-cd4-tdGFP* was a kind gift from Dr. Han Chun (Cornell University).

Imaging and Skeletonization

The larvae were mounted in 50% glycerol in PBS between a glass slide and a cover slip. The sample was imaged using a confocal laser scanning microscope (Zeiss, LSM780) with 63x objective. The 600x600 μm images were stitched together offline using Fiji and the stitched images were processed using the NeuronStudio [23] to obtain the skeleton a one pixel wide tracings of the dendritic arbors.

A Mathematical Definitions of Morphometrics

Radius of gyration of the Neuron

The radius of gyration is defined as

$$R_{\mathrm{g}} = \sqrt{\frac{1}{M}\sum_{j=1}^{M}(\mathbf{r}_j - \mathbf{r}_{\mathrm{m}})^2}, \tag{1}$$

where M is the total number of occupied pixels, $\mathbf{r}_j$ is the position of the j^{th} occupied pixel and $\mathbf{r}_{\mathrm{m}}$ is the mean position of all occupied pixels. R_{g} measures the standard deviation of the dendrite pixels, i.e., the spread of the imaged neuron from its center.

Path Correlation and Persistence Length

The deviation of a branch path from a straight line can be quantified using the tangent vector autocorrelation function

$$C_t(\Delta s) \sim \langle \hat{t}(s) \cdot \hat{t}(s + \Delta s) \rangle_s, \tag{2}$$

where $\hat{t}(s)$ is the tangent vector as a function of the path length s. C_t measures the angular change of the $\hat{t}$ as a function of path length, i.e., how bent the branch is. If $C_t = 1$, the path is straight and if $C_t = 0$, there is a 90^o turn in the path.

Branch Length Correlation Function

The branch length autocorrelation function is

$$C_l(\Delta d) = \frac{\langle L(d)L(d + \Delta d)\rangle_d - \langle L(d)\rangle_d^2}{\langle L^2(d)\rangle_d - \langle L(d)\rangle_d^2}, \tag{3}$$

where $L(d)$ is the branch length at depth d and Δd is the depth difference. Depth is defined as the number of branch points between the branch and the soma, along the shortest path from the branch to the soma. $\langle \ldots \rangle_d$ represents the average over d.

Hitting Probability

Consider a box with side length R centered anywhere in the receptor field of the neuron (Fig. 1 C). We then ask: 'what is the probability $P_H(b, R)$ of having b pixels in a box of size R?'. Using this probability, we can determine the probability that a box of size R contains at least n pixels

$$H_n(R) = \int_n^M P_H(b, R)\mathrm{d}b, \tag{4}$$

where M is the total number of neuron pixels. We define the mesh size B_{H} such that $H_1(R = B_{\mathrm{H}}) = 0.5$, i.e., the mesh size is the box width such that there is a 50% chance that the box contains at least one pixel from the skeleton.

Fractal Dimension

In this paper, the fractal dimension is measured using two different methods: the correlation dimension (Fig. 1 E) and box counting (Fig. 1 F) method. In the box counting method, we determine the number of boxes N of side length R that are needed to cover the neuron (Fig. 1 B). The number of boxes needed to cover a line of length l is $N = \frac{l}{R}$; therefore $N \propto R^{-1}$. The number of boxes needed to cover a square of side length l is $N = \left(\frac{l}{R}\right)^2$; therefore $N \propto R^{-2}$. In general, $N \propto R^{-d_\mathrm{b}}$, where d_b is the box counting measure of the fractal dimension.

In the correlation method [32], we determine how many pixels are contained within a circle of radius R. Let each point x_i on the neuron be the center of a circle of radius R (Fig. 1 B). Then $N(x_i, R)$ is the number of skeleton pixels in the circle (green pixels in Fig. 1 C). Averaging over all possible centers (i.e. skeleton pixels) x_i, gives

$$\kappa(R) = \langle N(x_i, R) \rangle_{x_i}. \tag{5}$$

In general, $\kappa(R) \propto R^{d_\mathrm{c}}$ where d_c is the correlation measure of the fractal dimension.

The relation $f(R) \propto R^d$ is called a scaling law and is only valid in a finite range of R (e.g. for small R we approach the scale of one pixel, and for large R we approach the total dimension of the neuron). For the neurons the minimum scale is half the mean branch length and the maximum scale is the radius of gyration.

Lacunarity

Consider the set of boxes of linear dimension R used in the box counting method (see figure 1 B). Instead of asking how many boxes are needed to cover the shape, we ask 'what is the probability $P_B(b, r)$ of having b pixels in a box of size R?'. $P_B(b, r)$ differs from $P_H(b, R)$ since it only considers boxes that have at least one pixel ($b \geq 1$).

The moments of P_B are defined as

$$\mu_n(R) = \int_1^M b^n P_B(b, R) \mathrm{d}b,$$

where M is the total number of skeleton pixels. This then allows us to look at the coefficient of variation of $P_B(b, R)$

$$CV(R) = \frac{\sigma^2}{\mu_1^2} = \frac{\mu_2 - \mu_1^2}{\mu_1^2}, \tag{6}$$

where σ^2 is the variance of $P_B(b, R)$. $CV(R)$ is also called the lacunarity function. The more uniform a shape is, the smaller CV and the more variable the shape, the larger the CV. For example, a uniform shape would have a $CV \sim 0$. How large CV needs to be for a shape/neuron to be consider variable is somewhat arbitrary. The more important point is that the larger CV, the larger the variation in the neuron. It also allows us to see how these variations change with length scale. Thus, the lacunarity function measures the variations and assigns them a typical length scale.

Acknowledgments

This work was partially supported by the NIH Pioneer Award (Award Number), National Natural Science Foundation of China (NSFC Grant 31671389, to X.L.) and Max-Planck Partner Program (to X.L.). SG was supported by an EMBO Long-Term Fellowship, and OT is supported by the Fonds de Reshershe du Qubec - Nature et technologies. Thanks to Dr. Han Chun (Cornell University) for the fly strains.

References

[1] Greg Stuart, Nelson Spruston, and Michael Häusser, editors. *Dendrites*. Oxford University Press, 2nd edition, 2007.

[2] D Bentley and A Toroian-Raymond. Embryonic and postembryonic morphogenesis of a grasshopper interneuron. *J Comp Neurol*, 201(4):507–18, Oct 1981.

[3] J W Truman and S E Reiss. Hormonal regulation of the shape of identified motoneurons in the moth manduca sexta. *J Neurosci*, 8(3):765–75, Mar 1988.

[4] Yan Li, Diana Brewer, Robert E Burke, and Giorgio A Ascoli. Developmental changes in spinal motoneuron dendrites in neonatal mice. *J Comp Neurol*, 483(3):304–17, Mar 2005.

[5] P F Hitchcock. Constant dendritic coverage by ganglion cells with growth of the goldfish's retina. *Vision Res*, 27(1):17–22, 1987.

[6] Jay Z Parrish, Peizhang Xu, Charles C Kim, Lily Yeh Jan, and Yuh Nung Jan. The microrna bantam functions in epithelial cells to regulate scaling growth of dendrite arbors in drosophila sensory neurons. *Neuron*, 63(6):788–802, Sep 2009.

[7] Rolf Bodmer and Yuh Nung Jan. Morphological differentiation of the embryonic peripheral neurons in drosophila. *Roux's archives of developmental biology*, 196(2):69–77, 1987.

[8] Richard Y Hwang, Lixian Zhong, Yifan Xu, Trevor Johnson, Feng Zhang, Karl Deisseroth, and W Daniel Tracey. Nociceptive neurons protect drosophila larvae from parasitoid wasps. *Curr Biol*, 17(24):2105–16, Dec 2007.

[9] H Wässle and B B Boycott. Functional architecture of the mammalian retina. *Physiol Rev*, 71(2):447–80, Apr 1991.

[10] M Häusser, N Spruston, and G J Stuart. Diversity and dynamics of dendritic signaling. *Science*, 290(5492):739–44, Oct 2000.

[11] D Attwell and S B Laughlin. An energy budget for signaling in the grey matter of the brain. *J Cereb Blood Flow Metab*, 21(10):1133–45, Oct 2001.

[12] Gordon M G Shepherd, Armen Stepanyants, Ingrid Bureau, Dmitri Chklovskii, and Karel Svoboda. Geometric and functional organization of cortical circuits. *Nat Neurosci*, 8(6):782–90, Jun 2005.

[13] Nelson Spruston. Pyramidal neurons: dendritic structure and synaptic integration. *Nat Rev Neurosci*, 9(3):206–21, Mar 2008.

[14] Quan Wen and Dmitri B Chklovskii. A cost-benefit analysis of neuronal morphology. *J Neurophysiol*, 99(5):2320–8, May 2008.

[15] Yuh-Nung Jan and Lily Yeh Jan. Branching out: mechanisms of dendritic arborization. *Nat Rev Neurosci*, 11(5):316–28, May 2010.

[16] S Lawrence Zipursky and Wesley B Grueber. The molecular basis of self-avoidance. *Annu Rev Neurosci*, 36:547–68, Jul 2013.

[17] Xintong Dong, Kang Shen, and Hannes E Bülow. Intrinsic and extrinsic mechanisms of dendritic morphogenesis. *Annu Rev Physiol*, 77:271–300, Feb 2015.

[18] Wesley B Grueber, Lily Y Jan, and Yuh Nung Jan. Tiling of the drosophila epidermis by multidendritic sensory neurons. *Development*, 129(12):2867–78, Jun 2002.

[19] Jessica L Robertson, Asako Tsubouchi, and W Daniel Tracey. Larval defense against attack from parasitoid wasps requires nociceptive neurons. *PLoS One*, 8(10):e78704, 2013.

[20] Benoit Mandelbrot. How long is the coast of britain? statistical self-similarity and fractional dimension. *Science*, 156(3775):636–638, 1967.

[21] Benoit B. Mandelbrot. *The fractal geometry of nature*. W.H. Freeman, 1 edition, August 1982.

[22] C. Allain and M. Cloitre. Characterizing the lacunarity of random and deterministic fractal sets. *Phys. Rev. A*, 44:3552–3558, Sep 1991.

[23] S L Wearne, A Rodriguez, D B Ehlenberger, A B Rocher, S C Henderson, and P R Hof. New techniques for imaging, digitization and analysis of three-dimensional neural morphology on multiple scales. *Neuroscience*, 136(3):661–80, 2005.

[24] Masao Doi and Sam F Edwards. *The theory of polymer dynamics*, volume 73. oxford university press, 1988.

[25] Zhiqiang Yan, Wei Zhang, Ye He, David Gorczyca, Yang Xiang, Li E Cheng, Shan Meltzer, Lily Yeh Jan, and Yuh Nung Jan. Drosophila nompc is a mechanotransduction channel subunit for gentle-touch sensation. *Nature*, 493(7431):221–5, Jan 2013.

[26] Michael Ashburner, Kent G Hawley Golic, et al. Drosophila: a laboratory handbook. Technical report, 2005.

[27] Benjamin J Matthews, Michelle E Kim, John J Flanagan, Daisuke Hattori, James C Clemens, S Lawrence Zipursky, and Wesley B Grueber. Dendrite self-avoidance is controlled by dscam. *Cell*, 129(3):593–604, May 2007.

[28] Peter Soba, Sijun Zhu, Kazuo Emoto, Susan Younger, Shun-Jen Yang, Hung-Hsiang Yu, Tzumin Lee, Lily Yeh Jan, and Yuh-Nung Jan. Drosophila sensory neurons require dscam for dendritic self-avoidance and proper dendritic field organization. *Neuron*, 54(3):403–16, May 2007.

[29] Katie M Hutchinson, Fernando Vonhoff, and Carsten Duch. Dscam1 is required for normal dendrite growth and branching but not for dendritic spacing in drosophila motoneurons. *J Neurosci*, 34(5):1924–31, Jan 2014.

[30] Benjamin J Matthews and Wesley B Grueber. Dscam1-mediated self-avoidance counters netrin-dependent targeting of dendrites in drosophila. *Curr Biol*, 21(17):1480–7, Sep 2011.

[31] Ian N Sneddon. The relation between load and penetration in the axisymmetric boussinesq problem for a punch of arbitrary profile. *International Journal of Engineering Science*, 3(1):47–57, 1965.

[32] Peter Grassberger and Itamar Procaccia. Measuring the strangeness of strange attractors. *Physica D: Nonlinear Phenomena*, 9(1–2):189 – 208, 1983.